https://dx.doi.org/10.21577/0103-5053.20220045

J. Braz. Chem. Soc., Vol. 33, No. 6, 509-522, 2022

Review

NMR Relaxometry Applied to Chemical Studies of Paramagnetic Metal Cation Complexes: Fundamentals and Applications

Flávio V. C. Kock [a,b]* ***and Luiz A. Colnago*** [c]

[a]*Departamento de Química, Universidade Federal de São Carlos, 13565-905 São Carlos-SP, Brazil*

[b]*Instituto de Química de São Carlos, Universidade de São Paulo, 13566-590 São Carlos-SP, Brazil*

[c]*Embrapa Instrumentação, 13560-570 São Carlos-SP, Brazil*

Low field time-domain nuclear magnetic resonance (TD-NMR) relaxometry of paramagnetic metal cations (PMC) has been widely used to study and improve contrast agents for magnetic resonance imaging (MRI). However, despite its remarkable potential, TD-NMR is rarely used to study PMC complexes, and coordination compounds in non-biomedical application. Therefore, this review aimed to provide comprehensive information not only to non-nuclear magnetic resonance (NMR) relaxation specialists, but also to scientists from distinct levels and expertise, as a way to pave the path for modern analytical and research of PMC complexes. Some fundamental concepts about NMR, paramagnetic relaxation mechanism, as well as traditional and modern methods to measure the longitudinal (T_1) and transverse (T_2) relaxation times constants are addressed. Here, we address some applications in analytical, electrochemical, and inorganic chemistry, electrodeposition reactions, as well as studies on PMC complexes and coordination compounds in solution.

Keywords: time-domain NMR, bench-top NMR, low-field NMR, NMR relaxometry, paramagnetic relaxation, analytical chemistry, inorganic chemistry, electrochemistry, coordination complexes

1. Introduction

Paramagnetic metal cations (PMC) containing one or more unpaired electrons in the d- or f-orbitals have important roles in living organisms, in chemical and pharmaceutical processes and in products and are widely used as contrast agents for magnetic resonance imaging (MRI) for diagnostic purposes.[1-4] In biology, Fe^{II}, Cu^{II}, Mn^{II}, Co^{II}, Ni^{II}, Mo^{III}, V^{II}, and other PMC, are normally coordinated to oxygen, nitrogen, or sulfur centers and are involved in several essential biological processes including mass and electron transports, enzymatic activities, among several other processes.[5]

PMC containing unpaired electrons, PMC complexes, and coordination compounds can be directly detected using electron spin resonance (ESR), also known as electron paramagnetic resonance (EPR).[6,7] They can also be indirectly detected by high-resolution nuclear magnetic resonance (HR-NMR) spectroscopy using their effects to enhance chemical shift dispersion (paramagnetic shift)[5,8,9] or to enhance relaxation processes.[10,11] However, the use of both EPR and HR-NMR requires expensive instrumentation, limiting their application in routine analysis, as well as at small universities and research facilities that do not have adequate instrumentation for these analyses.

This review shows how to obtain valuable information about PMC, complexes, and coordination compounds in solution using relaxometric measurements performed at low-cost, based on cryogen free, permanent magnets, and bench top low-field NMR instruments. The relaxometric analyses are normally performed in low (B_0 (static magnetic field) ca. 0.05 to 0.6 T) and inhomogeneous (ΔB_0 >> 10 ppm) magnetic field and directly in the time domain NMR (TD-NMR) signal, as no chemical shift information is observed. TD-NMR are affordable instruments when compared to superconducting high-resolution NMR spectrometers and can be useful method to obtain valuable structural, dynamical, and quantitative information on PMC in solution.

The TD-NMR relaxometers are a common analytical instrument used in several chemical areas where PMC are

*e-mail: kock.flavio@gmail.com
Editor handled this article: Humberto O. Stumpf (Associate)

important. Therefore, we present here a brief theory about the effect of PMC on longitudinal (T_1) and transverse (T_2) relaxation times constants, the pulse sequences used for measuring them, and the applications of TD-NMR relaxometry to obtain valuable information on PMC in solution, which are important in inorganic,[12] analytical,[13] electrochemistry[14] and coordination chemistry[15] studies.

2. Basic Theory about NMR Relaxation Times Constants

The NMR phenomenon is observed when a sample containing nuclei with spin quantum number (i.e., resulting spin magnetic moment) distinct from zero, is submitted to a static magnetic field B_0 (*z*-direction) and excited with a transverse oscillating (radiofrequency, rf) magnetic field B_1 (*xy*-plane). When a sample is placed in presence of B_0, the bulk of the magnetic moments collectively behaves as aligned to the *z*-direction (M_z) and reaches the Boltzmann energy distribution or the magnetization at thermal equilibrium (M_0). After a B_1 excitation the spins return exponentially to their thermal equilibrium losing energy to the environment (longitudinal relaxation) with a time constant (T_1) according to equation 1.

$$M_z = M_0\left(1 - e^{-\tau/T_1}\right) \quad (1)$$

where T_1 is the time constant of this exponential process known as longitudinal (*z*-direction) or spin-lattice relaxation time, and measured ranging specific delay times τ during the acquisition.

The spins also have a second relaxation process after B_1 excitation known as transverse (*xy*-plane) or spin-spin relaxation time or T_2. This process consists of losing its phase coherence in *xy*-plane, returning to a random distribution ($M_{xy} = 0$), with the time constant T_2 (equation 2).

$$M_{xy}(t) = M_0\left(e^{-t/T_2}\right) \quad (2)$$

Detailed mechanisms involved in T_1 and T_2 relaxation times constants are outside of the overview scope and can be found elsewhere.[7,16-21] Only the paramagnetic mechanisms are discussed here.

3. Effect of Paramagnetic Ion Complexes in Solvent Relaxation Time

The effect of paramagnetic ions in the relaxation times constants of the solvent nuclei was observed just after the discovery of the NMR phenomenon in 1946.[22] Bloch *et al.*[22] observed that the water longitudinal relaxation time (T_1) in aqueous solution of $Fe(NO_3)_3$ was much shorter than in distillated water.

The quantitative description of this effect was first described by Bloembergen, Purcell, and Pound[23] and improved by Solomon, Bloembergen, and Morgan from 1948 to 1966, known as the SBM heory.[24-26] According to these authors, the longitudinal (R_1) and transverse (R_2) relaxation rates of the solvent molecules, where $R_{1,2} = 1/T_{1,2}$, depend on the paramagnetic (R_p) and the diamagnetic (R_d) contribution, according to the equation 3:[1]

$$R_{i(obs)} = R_{i,p} + R_{i,d}, \text{ where } i = 1,2 \quad (3)$$

The R_p term is dominant in the relaxation mechanism for the solvent nuclei even when PMC are at very low concentration. R_p is directly proportional to paramagnetic ions concentration, [M], as described in equation 4:

$$R_i = [M] \times r_i \quad (4)$$

where r_i is the ^1H relaxivity and is expressed in units of mol L^{-1} s^{-1} while [M] is the PMC concentration in mol L^{-1}.[1]

The effect of paramagnetic ions on solvent relaxation is attributed to strong dipole-dipole interactions between the nuclear spin and the fluctuating local magnetic field of the unpaired electron spins in paramagnetic species.[1,27] R_{ip} contribution can be described using two components: contributions of the inner (IS) and outer (OS) spheres (equation 5).[1,27]

$$R_{i,p} = (R_{i,p})^{IS} + (R_{i,p})^{OS}, \text{ where } i = 1,2 \quad (5)$$

The IS and OS contributions account for the relaxation effects caused by the paramagnetic ion directly bound to the solvent molecules and the relaxation effect on the solvent molecules in the bulk, respectively. In addition, in more sophisticated models, other contributions have been considered, such as the second coordination sphere (SS), which concern solvent molecules kept close to the paramagnetic species by hydrogen bonds with hydrophilic groups on the ligand coordination cage.[1]

The inner-sphere (IS) term considers the exchange between the water molecule(s) directly coordinated to the paramagnetic ion and the solvent ions to propagate the paramagnetic effect to the bulk. In particular, the relaxivity of bulk water hydrogens can be described according to equation 6:[1,27]

$$(R_i)^{IS} = \frac{q \times P_M}{T_{1M} + \tau_M}, \text{ where } i = 1,2 \quad (6)$$

where: q represents the number of water molecules directly coordinated to paramagnetic species, P_M is the mole fraction of bound solvent nuclei, τ_M corresponds to residence lifetime for the solvent molecule in the first coordination sphere, and T_{1M} represents the proton longitudinal relaxation rate for the coordinated solvent molecule.

Therefore, from the SBM theory, in a fast exchange regime for the solvent molecules ($\tau_M << T_{1M}$), the paramagnetic effect experienced by the solvent molecules far from the paramagnetic ion is equal to that experienced by the solvent molecules directly coordinated to paramagnetic species.[27] In addition, based on equation 7, T_{1M} can be described by a scalar (SC) (by the chemical bond) and a dipolar (DD) (spatial) component. In the presence of a paramagnetic coordination complex, the dipolar term has a higher predominance, due to the $1/r^3$ dependence of the energy ($1/r^6$ in the relaxation) associated to this term.[1,27]

$$1/T_{iM} = R_{TiM} = (R_{Ti})^{DD} + (R_{Ti})^{SC}, \text{ where i = 1,2} \quad (7)$$

On the other hand, dipole-dipole interactions are governed by a set of parameters, summarized in equation 8:[27]

$$R_1^{DD} = \frac{2}{15}\frac{\gamma_I^2 g^2 \mu_B^2 S(S+1)}{r^6}\left[\frac{3\tau_{c1}}{\left(1+\omega_I^2\tau_c^2\right)} + \frac{7\tau_{c2}}{\left(1+\omega_S^2\tau_c^2\right)}\right] \quad (8)$$

where: γ_I and g correspond to the nuclear gyromagnetic ratio and the electron spin g-factor, respectively; μ_B is the Bohr magneton, S is the spin quantum number for the paramagnetic species (e.g., S = 1/2 for Cu^{II} and 7/2 for Gd^{III}), τ_c is the correlation time, r is the electron spin-proton distance, and ω_I and ω_S are the proton and electron Larmor precession frequencies, respectively.[1,27]

Furthermore, the characteristic correlation time τ_c is supported by multiple molecular dynamic processes, such as the rotational correlation time (τ_R), which means the time needed for the reorientation of the paramagnetic ion-proton vector, the water residence time in the first coordination sphere (τ_M) and the longitudinal (T_{1e}) and transverse (T_{2e}) electronic relaxation times constants for the metal ion, in agreement to equation 9.[27]

$$\frac{1}{\tau_c} = \frac{1}{\tau_R} + \frac{1}{\tau_M} + \frac{1}{T_{ie}}, \text{ where i = 1,2} \quad (9)$$

More detailed quantitative information about the effect of paramagnetic species on the relaxation solvent nuclei can be found elsewhere.[1,7,17,27]

4. Pulses Sequences to Measure Longitudinal (T_1) and Transverse (T_2) Relaxation Times Constants

4.1. Pulse sequences to measure T_1

T_1 is the time constant related to the time taken by a collection of spins to exponentially recover their magnetization along M_z after B_1 excitation. Several pulse sequences have been developed to measure T_1, such as inversion-recovery (IR), saturation-recovery (SR), progressive saturation (PS), among others.[28-31] IR is the standard pulse sequence to measure T_1 and uses a π pulse to invert magnetization, followed by time (τ), $\pi/2$ pulse, and a recycle delay $\geq 5T_1$, which is the time to restore at least 99.33% of M_0.

The IR curve is obtained by measuring the free induction decay (FID) intensity, after the $\pi/2$ pulse, as function of several delay times τ. Figure 1 shows FID intensity variation for a 0.25 mM aqueous solution of $MnSO_4$, as function of logarithmically space τ values. For τ equals to zero or much shorter than T_1, FID intensity is negative. FID intensity is zero (null point) when $\tau = \ln 2\, T_1$. For longer τ values, FID intensity is positive and reaches a maximum for τ values $\geq 5T_1$. The null point is used as a fast estimation of T_1 value; however, a precise or multiple relaxation time measurements requires fitting the data with an exponential function or using inverse Laplace transformation.[32,33] One of the drawbacks of the IR sequence is the long time to perform the measurements, as it requires at least a time $\geq 5T_1$ between repetitions and a single data point is collected in each scan.

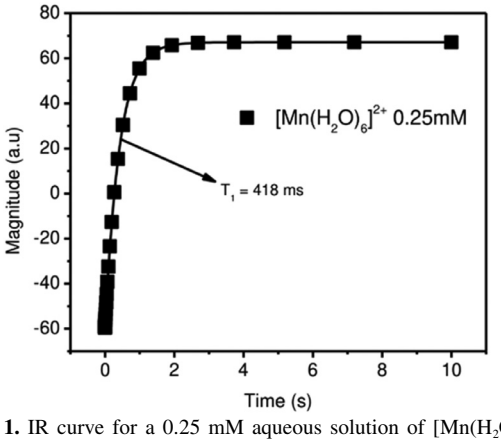

Figure 1. IR curve for a 0.25 mM aqueous solution of $[Mn(H_2O)_6]^{2+}$ complex. The value of T_1 = 418 ms was obtained by fitting the experimental data using a mono exponential function.

The SR and PS pulse sequences can reduce the experimental time to measure T_1, as these sequences do not require to wait for $5T_1$ recycle delay. Recently, fast methods

to measure T_1 using single shot sequences based on the continuous wave free precession regime (CWFP-T_1) and driven-equilibrium principles, named small-angle flip-flop (SAFF) pulse sequences have been proposed.[34,35]

4.2. Pulse sequences to measure T_2

T_2 is an exponential process related to the time taken by a collection of nuclei to lose their phase coherence after rf excitation and return to a random distribution in the *xy*-(transverse) plane. T_2 is the time constant of this process (equation 2) and is only observed in FID acquired in perfectly homogeneous magnet. In existent magnets, especially in the inhomogeneous magnets used in TD-NMR equipment, the FID time constant is far from the sample T_2 value. The effective transverse relaxation time of FID (T_2*) depends on T_2 and magnetic field inhomogeneity (ΔB_0), according to equation 10.[21]

$$\frac{1}{T_2^*} = \frac{1}{T_2} + \frac{1}{T_{2_{(\Delta B_0)}}} \quad (10)$$

To obtain the value of sample T_2, regardless of the magnetic field inhomogeneity, Hahn[36] proposed a spin-echo sequence consisting of two $\pi/2$ pulses separated by time τ. This sequence refocuses a spin echo signal and its amplitude at 2τ, from the first pulse, is maximum, restoring the phase coherence lost, due to the magnetic field inhomogeneity. To obtain the full T_2 relaxation curve, it is necessary to perform several spin echo measurements as a function of the time (τ) similarly to IR.

Carr and Purcell[37] proposed two more efficient pulse sequences, similar to those proposed by Hahn,[36] replacing the second pulse by π pulse. However, both sequences cannot be used to measure T_2 of liquid or solution in inhomogeneous magnets due to interference of molecular self-diffusion in the spin echo intensity for long τ values. To overcome this limitation, Carr and Purcell[37] proposed a single shot sequence to measure the full echoes decay in one experiment using constant and short τ values, known as CP (Carr-Purcell) sequence. This single shot sequence uses a $\pi/2$ pulse separated by a constant τ value and a train of π pulses separated by a constant 2τ value. One of the main drawbacks of the single shot CP sequence is its strong dependence on accurate π pulses. To solve this problem, Meiboom and Gill[38] introduced a 90° phase shift between the first $\pi/2$ (*x* axis) and the π pulses (*y* axis). This phase shift makes the sequence very robust and a refocusing pulse as short as $\pi/2$ can be used to obtain accurate T_2 values.[39,40] Therefore, the CP sequence improved by Meiboom-Gill, known as CPMG, is the standard method to measure T_2. The maximum amplitude of the echoes in function of time (Figure 2) is used to obtain the T_2 values by mono or multi-exponential fitting or by inverse Laplace transform methods.[38]

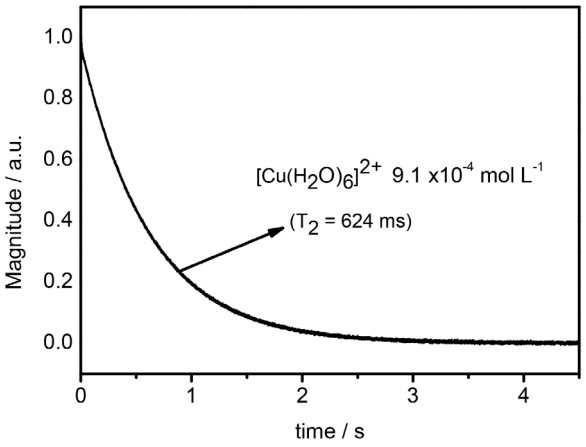

Figure 2. CPMG decay curve for the aqueous solution of $[Cu(H_2O)_6]^{2+}$ complex (9.1×10^{-4} mol L^{-1}). The value for T_2 = 624 ms was obtained by a mono exponential fitting.

4.3. Single shot pulse sequences to measure T_1 and T_2 in single experiment

Longitudinal and transverse relaxation times constants are governed by different mechanisms and their ratio (T_1/T_2) can be as low as 1 for liquid or non-viscous diamagnetic solutions for more than one order of magnitude, even in non-viscous solutions, containing paramagnetic ions complexes.[41]

Three single shot pulse sequences have been proposed to measure T_1 and T_2 in single experiment, based on the continuous wave free precession (CWFP) regime. The CWFP is a special condition of the steady state free precession (SSFP) regime.[42,43] Ernst and Anderson[44] described quantitatively the SSFP regime by using the Bloch equation.[42-45] The SSFP regime is obtained when the sample is irradiated with a train of rf pulse with constant repetition time (T_p) shorter than T_2 (T_p ca. T_2). In this sequence, an FID and a spin echo signal are observed, before and after each rf pulse. These two signals usually do not overlap and are used to obtain fast magnetic resonance imaging as well as fast high resolution NMR spectrum.[42,46-48]

Conversely, the CWFP regime is observed when the pulse is repeated with time T_p shorter than the effective transverse relaxation time T_2* ($T_p < T_2$*).[42,43,45] In this regime, a strong interaction between FID and spin echo signal is observed, forming a signal with constant amplitude (CWFP). When the FID-echo interaction is constructive, a maximum signal is observed; conversely, when the FID-eco interaction is destructive, a signal with minimal amplitude is observed. The theory for the CWFP regime has been discussed elsewhere[42,49,50] and will not be discussed in detail here.

Venâncio *et al*.[51] shows for the first time that the CWFP sequence can be used to measure T_1 and T_2 in a single shot experiment. Figure 3 shows the time evolution CWFP signal from the first pulse to the CWFP regime, using $\pi/2$ pulse, $T_p < 1/2\ T_2$*, and an odd precession angle (ψ) for a constructive interference. After the first pulse, the amplitude of the NMR signal is maximum and proportional to the initial magnetization (M_0). After the following pulses, the signal shows strong oscillation and decays to a *quasi*-stationary state (QSS). The QSS state is observed when the strong oscillations stop and the signal decays exponentially with a time constant T^* to reach the CWFP signal with constant amplitude (M_{SS}).

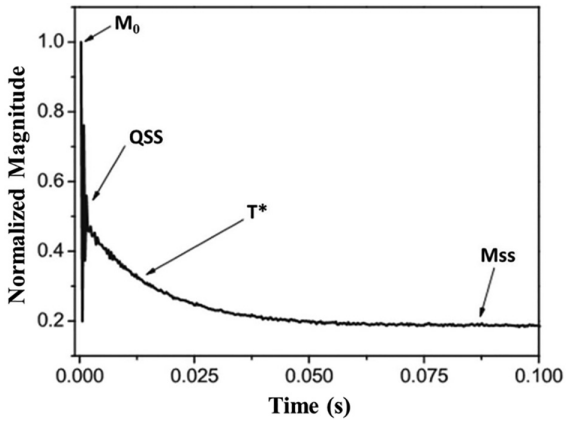

Figure 3. NMR magnitude signal obtained with the CWFP pulse sequences, highlighting the parameters M_0, M_{SS}, and T^* used to determine T_1 and T_2 (reproduced from reference 41 with copyright permission from Elsevier B.V.).

The M_{SS} amplitude and T^* values obtained with the CWFP sequences are dependent on both relaxation times constants (T_1 and T_2) and M_0, according to equations 11 and 12:[40,42,45]

$$M_{SS} = \frac{M_0 \times T_2}{(T_1 + T_2)} \tag{11}$$

$$T^* = \frac{2 \times T_1 \times T_2}{T_1 + T_2} \tag{12}$$

Rearranging these equations to equations 13 and 14 allows calculating T_1 and T_2 using the experimental values of M_0, M_{SS}, and T^*.[40,42]

$$T_1 = \frac{T^*/2}{M_{SS}/M_0} \tag{13}$$

$$T_2 = \frac{T^*/2}{1-(M_{SS}/M_0)} \tag{14}$$

One of the limitations of the CWFP sequence is the low dynamic range (DR) of the T^* decay for an adequate exponential fitting, when T_1/T_2 ca. 1 (Figure 4a). A second pulse sequence was developed to overcome this limitation, introducing a time delay of $\tau/2$ between the first and second pulses, named the Carr-Purcell CWFP (CP-CWFP) sequence.[40] This sequence allows obtaining a maximum DR for time T^* for samples with T_1/T_2 ca. 1, Figure 4b. However, the sequence has low DR for sample $T_1 >> T_2$ (Figure 4b).

Therefore, a third CWFP pulse sequence was developed to obtain high DR, independence at the T_1/T_2 ratio (Figure 4c) and use a precession angle (ψ) equals to zero, that is, the experiment can be performed on resonance and independently of T_p.[52] This new sequence with 180° phase shift alternation, was named CP-CWFPx-x.[49,52-54]

4.4. Two-dimension pulse sequences for measuring T_1 and T_2 correlation

When the relaxation curve shows a multiexponential behavior (multiples T_1 or T_2), it is not possible to know how T_1 correlates with each T_2. Multiple relaxation times constants are normally observed in compartmentalized,

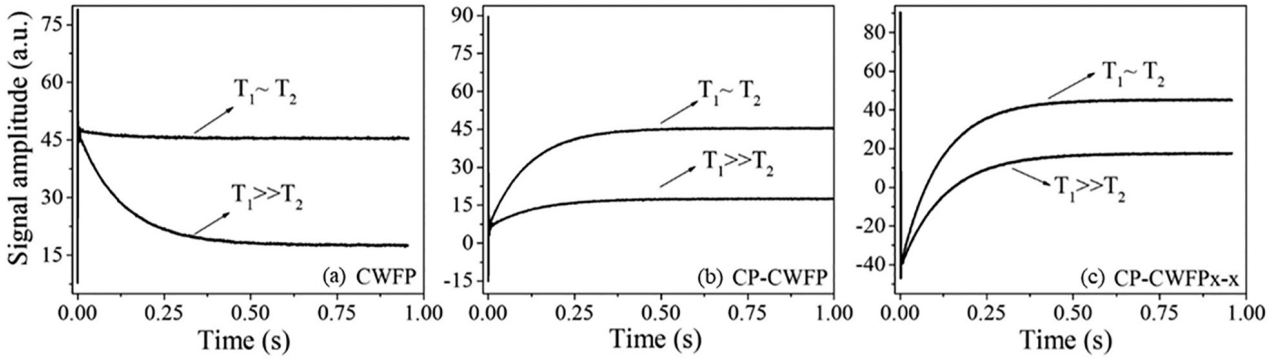

Figure 4. Experimental (a) CWFP; (b) CP-CWFP and (c) CP-CWFPx-x signals for solutions of 10 mM $CuSO_4$ ($T_1 = T_2$) and 1 mM $MnSO_4$ ($T_1 >> T_2$), demonstrating clearly the long dynamic range obtained for the sequence CP-CWFP$_{x\text{-}x}$, which allows a more reliable fitting for experimental data for any T_1/T_2 ratio (figure from reference 49 with CC-BY attribution).

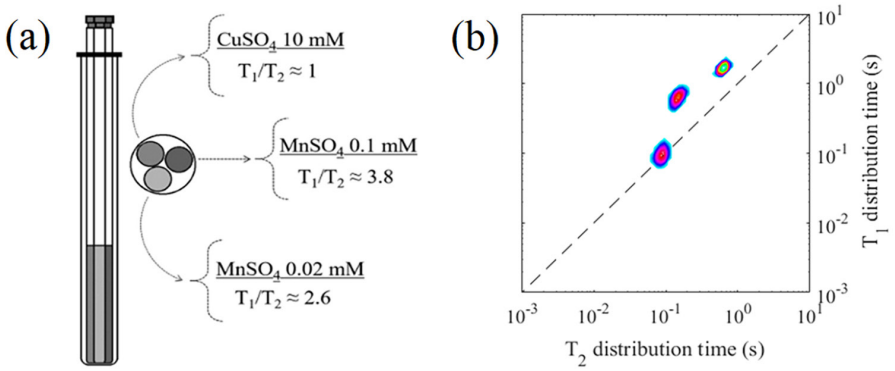

Figure 5. (a) Phantom sample composed by three 3 mm NMR tubes inserted in a 10 mm NMR tube. The gray tone in the circle/tubes represents a different aqueous solution: 10 mM $CuSO_4$, 0.1 mM $MnSO_4$, and 0.02 mM $MnSO_4$; (b) 2D T_1-T_2 correlation map obtained with the sample of Figure 5a (adapted from reference 57).

porous, or emulsion samples. To obtain the correlation between T_1 and T_2, it is necessary to use 2D pulses sequences composed by a T_1 and T_2 pulse sequences, such as IR-CPMG, SR-CPMG, or CPMG-CWFP-T_1.[49,55,56]

Figure 5 shows the T_1-T_2 correlation maps of three compartmentalized aqueous solutions of paramagnetic ions (Figure 5a). The 2D correlation map (Figure 5b) shows the three T_1 and T_2 values and the correlation between them. These 2D relaxometric studies can be a valuable tool for research on paramagnetic ions in heterogeneous environments, such as porous inorganic media or biological tissues.[57]

5. Applications of TD-NMR Relaxometry in Systems Containing Paramagnetic Ions

This section describes how it is possible to extract quantitative, structural, and dynamical information about PMC and PMC complexes and coordination compounds in solution, using low-field bench-top TD-NMR relaxometry. The applications of PMC in MRI contrast agents are outside the scope of this review and can be found elsewhere.[1,2,58,59]

5.1. Applications in analytical chemistry

The longitudinal relaxation rate ($R_1 = 1/T_1$) of the solvent is influenced by the paramagnetic ions concentration (mol L^{-1}) and its effective electronic magnetic moment (μ_{eff}), the nucleus gyromagnetic ratio γ, Boltzmann constant k, sample temperature (T) and sample viscosity (η), and is calculated according to equation 15.[22,23]

$$\frac{1}{T_1} = \frac{12\pi^2\gamma_P^2\eta[M]\mu_{eff}^2}{5kT} \quad (15)$$

Therefore, R_1 has a linear correlation to paramagnetic ion concentration for the sample with the same temperature and viscosity.[22,23]

The use of NMR relaxometry for quantitative analyses of PMC in solution was first demonstrated in 1970's. Nothnagel and Weiss[60] and Schluter and Weiss[61-63] demonstrated the use of T_1, measured with IR pulse sequence, to monitor precipitation and complexation of paramagnetic ions by NMR titration in aqueous solutions. The authors also observed that the transverse relaxation rate ($R_2 = 1/T_2$) has similar linear correlation with the PMC concentration in solution.

Currently, T_2 are frequently used in relaxation analyses because its measurement using CPMG pulse sequence is much faster than T_1 measurement using IR sequence.[64,65] Figure 6 shows the linear correlation of R_2 and the concentration of several PMC in aqueous solution. The curve slope corresponds to molar relaxivity (equation 4) that depends on μ_{eff} and it is maximum for the Mn^{II} and minimal for Cu^{II} (Figure 6). These differences can be attributed to the number of unpaired electrons on the d-orbitals, 5 unpaired electrons (d^5), and 1 unpaired electron (d^9) for Mn^{II} and Cu^{II} ions, respectively,

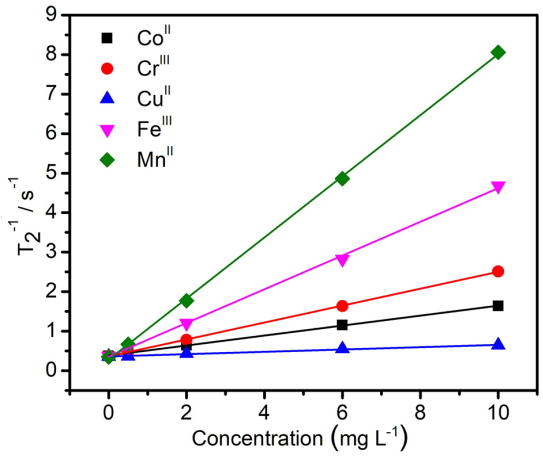

Figure 6. Variation of the transverse relaxation rate (T_2^{-1}) of water *versus* the concentrations of Co^{II}, Cr^{III}, Cu^{II}, Fe^{III} and Mn^{II} in the solutions (reproduced from reference 65 with copyright permission of Elsevier B.V.).

and the ability of the metal to energetically split the d-orbitals.[66,67]

The R_2 determination is fast (seconds) and CPMG is a non-destructive method that can be a useful alternative analytical approach to measure PMC concentrations in solution, as demonstrated by Gomes *et al.*,[68] with low limits of detection (LOD ca. 10^{-6} mol L^{-1}) and quantification (LOQ ca. 10^{-5} mol L^{-1}). Furthermore, the highest sensitivity was observed for Mn^{II} ions (LOQ ca. 10^{-6} mol L^{-1}), which can be associated to a larger number of unpaired electrons, a positive feature, enhancing the relaxation effect.[68]

In 2018, Kock *et al.*[65] and Gomes *et al.*,[68] using 2 and 9 MHz (for ^1H nucleus) relaxometers, respectively, demonstrated that TD-NMR T_2 relaxometry was a simple, rapid, and efficient method to determine PMC concentrations in aqueous solution. The high correlation observed with inductively coupled plasma optical emission spectrometry (ICP OES) (Figure 7) shows that T_2 relaxometry even at 2 MHz is a cost-effective alternative to quantify PMC at small enterprises and universities.[65]

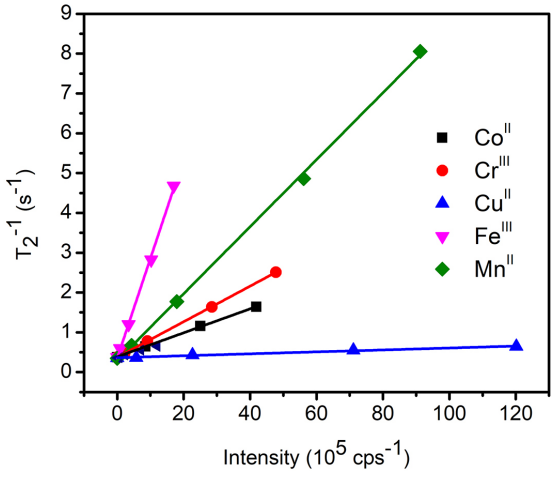

Figure 7. Correlation between transverse relaxation rates (T_2^{-1}) obtained from TD-NMR relaxometry *versus* optical emission intensity obtained from ICP OES: Co^{II}, Cr^{III}, Fe^{III}, Cu^{II}, and Mn^{II} (reproduced from reference 65 with copyright permission of Elsevier B.V.).

In 2015, Cobra *et al.*[69] used the TD-NMR T_2 relaxometry to determine the solubility product constant (K_{sp}) for several salts containing paramagnetic ions in aqueous solution. In these experiments, R_2 was measured as function of pH and the PMC concentrations were determined to calculate K_{sp}. The authors also showed that it is possible to separate different paramagnetic ions by precipitation (Figure 8) as a function of pH. The three steps sigmoidal curves are related to Fe^{III} precipitation at pH 3.04, Cu^{II} at pH 7.70, and Mn^{II} at pH 9.40.[69]

TD-NMR relaxometry have also been used to determine Mn^{2+} ions in wine samples,[70] characterization

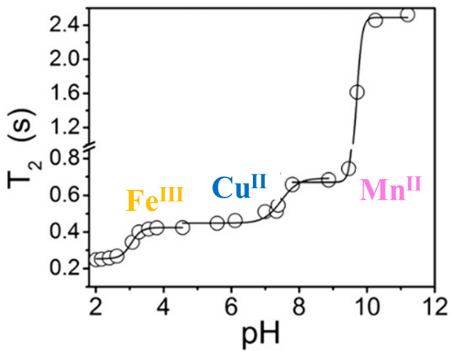

Figure 8. Experimental relaxometric titration curves showing the variation of T_2 with the pH for an aqueous solution containing $FeCl_3$, $CuSO_4$, and $MnSO_4$ (reproduced from reference 69 with copyright permission of Elsevier B.V.).

of polymer materials doped with paramagnetic ions for the development of the product and the process in several industries, namely rubber, plastics, composites, adhesives.[71] TD-NMR relaxometry has also been used as an indicator of black heart problem in pomegranate fruits, diseases caused by the high amount of PMC, such as Mn^{2+} ions.[72]

5.2. Applications in electrochemistry

T_2 measurements with the CPMG pulse sequence have been successfully used to monitor Cu electrodeposition reactions *in situ* or *in operando*. The first electrodeposition experiment measured with T_2 relaxometry was performed in the Cu^{II}-sorbitol complex $[Cu(Sorbitol)_2]^{2.}$[73] Cu^{II} electrodeposition has been monitored using different TD-NMR apparatus, probes with inductively coupled coils.[74]

Figure 9a shows the setup for the Cu^{II} electrodeposition experiment. The working (WE), reference (RE) and counter (CE) electrodes were inserted into the NMR probe and the measurements were performed *in operando*. Figure 9b shows the variation of Cu^{II} concentration as a function of electrodeposition reaction time and the respective electric density current (**j**) variation.

When the same Cu^{II} electrodeposition reaction was performed *ex situ* (in the absence of a magnetic field) and *in situ* (in the presence of NMR magnetic field), the *in situ* reaction was faster than the *ex situ* reaction (Figure 10a).[13,74,76] In the *ex situ* experiments, the electrochemical system was placed in the NMR relaxometer for a few seconds only to measure the Cu^{II} concentration using the CPMG sequence. In the *in situ* experiments, the electrochemical cell stays in the magnetic field during the entire reaction time.

The increase in the reaction rate (Figure 10a) was attributed to the magnetohydrodynamic effect (MHD)[77] that was observed when the electrochemical reaction was

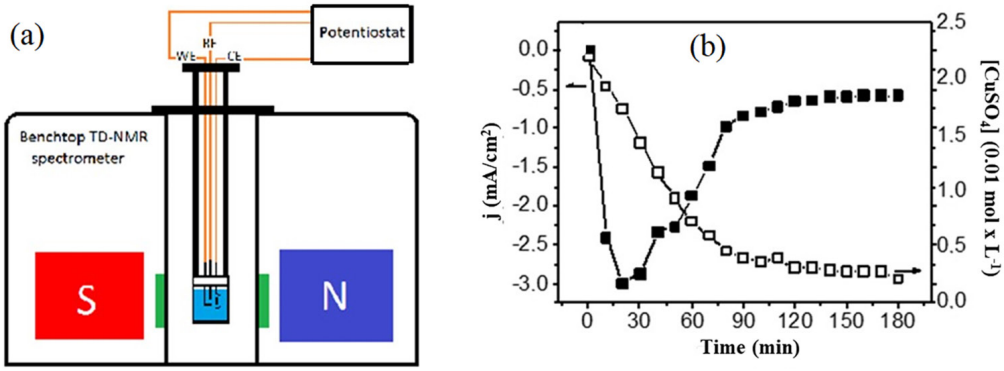

Figure 9. (a) Representation for the *in situ* electrochemistry system coupled to TD-NMR benchtop spectrometer; (b) variation of Cu^{II} concentration (□) and potentiostat current (■) during the electrodeposition reaction (reproduced from Nunes *et al.*,[75] with copyright permission 2022 from American Chemical Society).

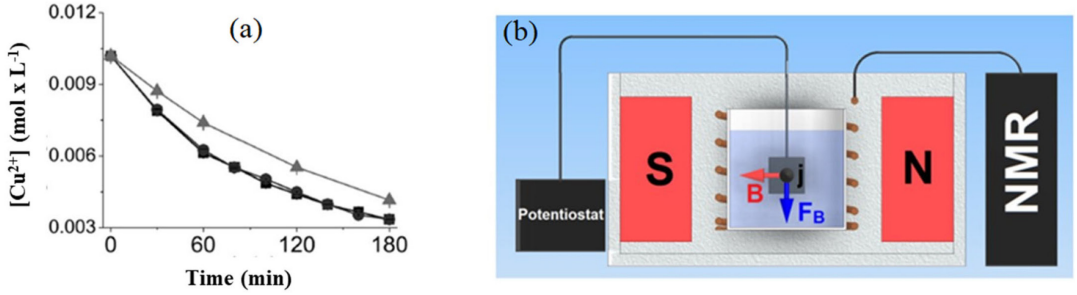

Figure 10. (a) Variation of Cu^{II} concentration as a function of electrolysis time performed in the electrochemical cell recorded at 23 °C under different configurations: (■) $\mathbf{B} \perp \mathbf{j}$, (●) $\mathbf{B} \parallel \mathbf{j}$, and (▲) $\mathbf{B} = 0$. Solution: 0.1 M Na_2SO_4 electrolyte containing 0.01 M $CuSO_4$. Conditions: $E_{applied} = -0.4$ V *vs.* Ag/AgCl (3 mol L^{-1} KCl) (figure from reference 14 with CC-BY attribution); (b) illustration of the electrochemical cell inserted in the NMR relaxometer (0.23 T). $\mathbf{F_B}$ is the magnetohydrodynamic force (integral force density acting on all species in solution) that is the cross product between the current density (**j**) and the magnetic induction (**B**), which produces a force perpendicular to both vectors ($\mathbf{F_B} = \mathbf{j} \times \mathbf{B}$). Therefore, the resultant force generates a flow in the solution, increasing mass transport (figure from reference 13 with CC-BY attribution).

performed in the presence of a magnetic field. The main MHD force is the Lorentz force ($\mathbf{F_L}$) that is equal to the cross product to magnetic field strength (**B**) and ionic density current (**j**). This force acts on the solution medium stirring it. $\mathbf{F_L}$ is maximum when **B** and **j** are perpendicular ($\mathbf{B} \perp \mathbf{j}$) and minimal for **B** and **j** parallel ($\mathbf{B} \parallel \mathbf{j}$). However, no difference between both orientations were observed (Figure 10a) due to distortions in the electric and magnetic fields.[13,74,76] This mass transport phenomenon observed during Cu^{II} electrodeposition in NMR magnetic field was measured *in situ* by magnetic resonance imaging velocimetry.[78]

5.3. Applications in inorganic chemistry

TD-NMR relaxation measurements have also been used to study PMC complexes and coordination compounds. In 2015, Kock and Colnago[41] studied the Cu^{II}-EDTA (ethylenediamine tetra acetic acid) complex as a function of the pH (Figure 11a) measuring T_1 and T_2, simultaneously, using the CWFP and CP-CWFP pulses sequences. Figure 11a (solid lines) shows relaxation times constants and visible absorption profiles of the Cu^{II}-EDTA complex, as a function of the pH. The solid lines are the polynomials fit of T_1 (☆), T_2 (○), and absorption at 730 nm (■) (visible spectroscopy) data. The dashed line is the sigmoidal fit to T_2 values (□) of the Cu^{II} solution without EDTA. These results clearly show the strong influence of the EDTA complex on relaxation profile of Cu^{II} solution, when compared with the solution without Cu^{II}. These results also show how similar are the absorbance and the relaxation times constants profiles for the Cu^{II}-EDTA complex, as a function of the pH (Figure 11a). These similar profiles have been explained through the progressive ligand replacing the inner coordination sphere from aqua $[Cu(H_2O)_6]^{2+}$ to $[CuY]^{2-}$ (Figure 11b). The authors suggested that the EDTA ligand influences the paramagnetic effect on the solvent relaxation time, demonstrated by ^{1}H-relaxometry, and that the chemical equilibrium is shifted for the formation of the chelate species in solution.[41,79]

However, a much different profile between T_1 and T_2 relaxation and absorption at 730 nm is observed when the Cu^{2+}-EDTA complex is in the presence of NH_4OH (Figure 12). The relaxation profiles show two peaks while the absorption profile shows only one broad peak.[41] The chemical structures differences between the Cu^{II}-EDTA and Cu^{II}-EDTA plus NH_4OH, as a function of the pH,

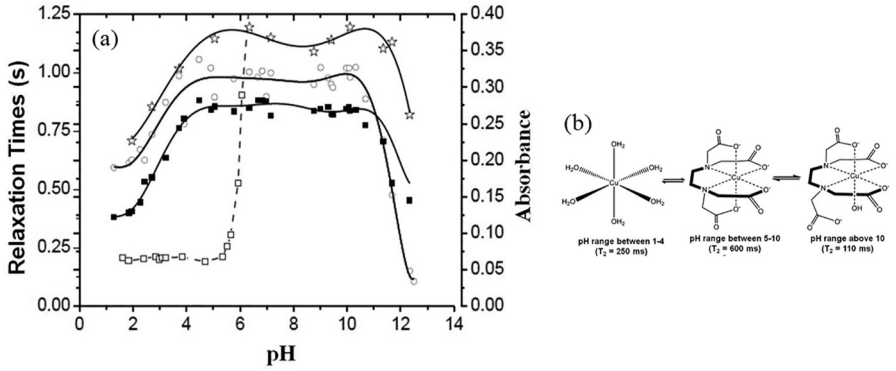

Figure 11. (a) Variation of maximum absorbance at 730 nm (■), T_1 (☆), and T_2 (○) measured simultaneously with the CP-CWFP pulse sequence for the aqueous solution of complex $[CuY]^{2-}$ and T_2 measured with CPMG (□) for the aqueous solution of Cu^{II}, as a function of the pH; (b) proposed complex species as a function of the pH obtained from the aquocomplex $[Cu(H_2O)_6]^{2+}$ to hydroxo complex species, $[Cu(Y)OH]^{3-}$ (adapted from reference 41).

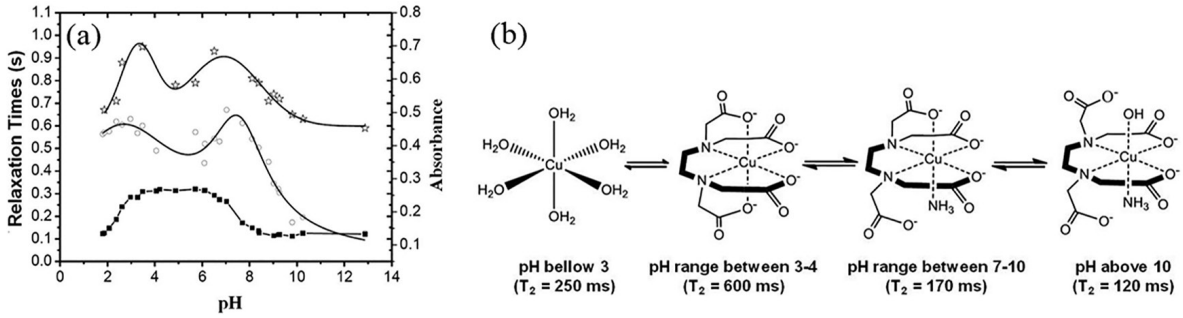

Figure 12. (a) Variation of maximum absorbance at 730 nm (■), T_1 (☆) and T_2 (○) measured simultaneously by CP-CWFP pulse sequence for the aqueous solution in the presence of $(NH_4)_2SO_4$ (1.0 mol L^{-1}) of complex Cu^{II}-EDTA in function of pH. In all experiments the Cu^{II} concentration was 3.3×10^{-3} mol L^{-1}; (b) proposed complex species as a function of the pH obtained from the aquocomplex $[Cu(H_2O)_6]^{2+}$ to amino hydroxo complex $[Cu(Y)(NH_3)OH]^{3-}$ species (adapted from reference 41).

are shown in Figure 12b. Therefore, both relaxation times constants obtained using rapid and simultaneous CWFP and CP-CWFP pulses sequences can be efficient to study metal complexes containing paramagnetic ions, as an alternative to traditional UV-Vis spectrophotometry. Besides, TD-NMR relaxometry can be used to study colorless complexes, such as Mn^{II}-EDTA,[41] which is not possible with the use of visible spectrophotometry.

The CWFP pulse sequences were also used to study the interaction between the biopolymer chitosan and paramagnetic ions.[54] Figures 13a and 13b show the relaxometric profiles of an aqueous solution of chitosan (CHI), in the presence and absence of the paramagnetic Fe^{III}, as a function of the pH, respectively.[53,54] These results highlighted that the relaxation profiles of both solutions are remarkably different, especially under alkaline conditions, suggesting a strong interference of this biopolymer and its respective chelate $[CHI\text{-}Fe]^{3+}$ (Figure 13c)[80] on water mobility due to the coagulation process, which, in practical terms, concerns the removal of these heavy metals from solution.[53]

These results demonstrate that the CWFP pulse sequences could be used to study the interactions of paramagnetic ions and other CHI molecules with different molecular weights, acetylation degrees, and derivatives, as well as between other water-soluble polysaccharides and paramagnetic ions, providing a distinct perspective on the CHI-metal binding properties and stability in solution, commonly studied by other expensive and laborious analytical approaches, such as atomic absorption spectrometry (AAS)[81,82] and ICP OES.[83] Therefore, TD-NMR is an interesting alternative for the studies on the interaction between macromolecules and metals ions, with significant impact on bioinorganic,[5] environmental chemistry,[84] as well as for the development of novel functionalized materials.[85]

Another interesting result was obtained for the Cu^{II}-sorbitol complex, $[Cu(Sorbitol)_2]^{2-}$, used in numerous technological applications.[73,86] Figure 14a shows the T_1 and T_2 relaxometric profiles obtained with the CP-$CWFP_{x\text{-}x}$ pulse sequence. This figure shows that the relaxation times constants for this complex are remarkably distinct for a pH above 6. The T_1 curve shows that the Cu^{II} has no influence on bulk water, similar to what is observed in pure water. On the other hand, the T_2 profile shows that the $[Cu(Sorbitol)_2]^{2-}$ species is totally formed at pH ca. 12

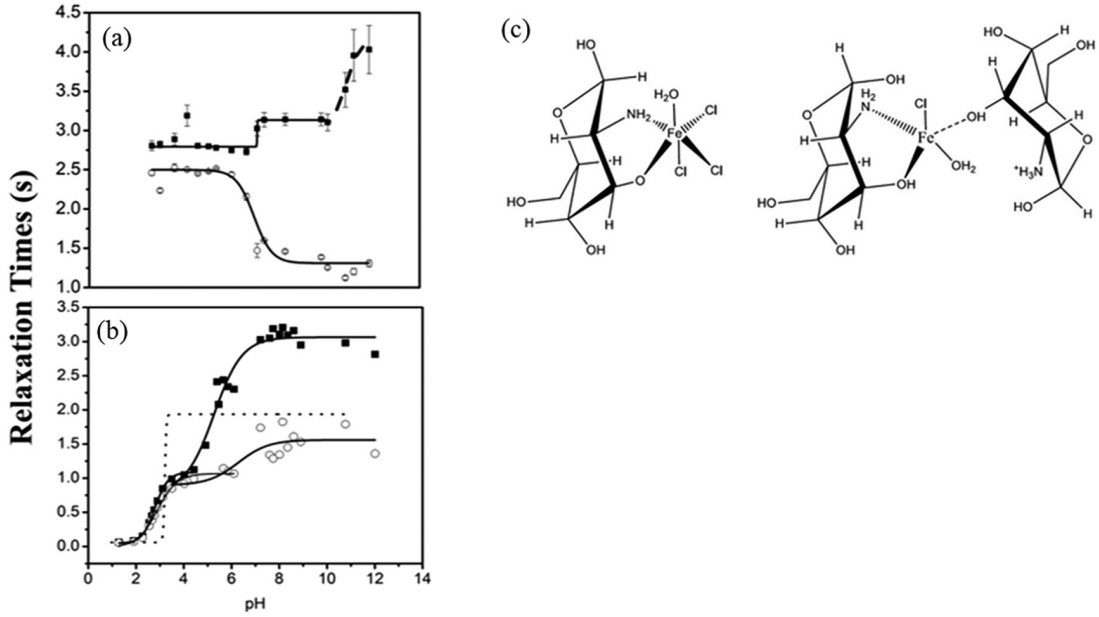

Figure 13. T_1 (■) and T_2 (○) relaxometric profiles obtained for a chitosan aqueous solution (a) and for $[CHI\text{-}Fe]^{3+}$ (b) using the CP-CWFP$_{x\text{-}x}$ pulse sequence; (c) proposed chemical arrangements for the $[CHI\text{-}Fe]^{3+}$ species[54,80] (figures adapted from references 53, 54 and 80).

(blue arrow), where neither paramagnetic nor viscosity effect influences the relaxation mechanisms.[87] At other pH values above 6, the T_2 values indicate that the complex alters the solution viscosity. Therefore, the absence of a paramagnetic effect on both T_1 and T_2 at pH ca. 12 indicates that water molecules do not have access to Cu^{II} ions and consequently that the Cu^{II} ions are wrapped in the soluble complex toroidal structure (Figure 14b),[86] in a supramolecular arrangement, as suggested by X-ray diffraction composed by 8 sorbitol molecules and 16 Cu^{II} ions, and now confirmed by TD-NMR relaxometry that they occur in solution.[87]

Furthermore, TD-NMR relaxometry has been used in inorganic chemistry to monitor the Cr^{VI} photocatalytic reduction performance by quantifying the concentration of paramagnetic Cr^{III} ions in solution,[88] the removal of Cu^{II} and Cr^{III} ions from water by amberlite IR120 resin,[89] and adsorption research of Cu^{II} on activated alumina.[90] Table 1 presents additional applications of TD-NMR relaxometry to PMC, concerning the analytical and inorganic chemistry.

6. Final Remarks

This review demonstrated the potential use of NMR relaxometry to study paramagnetic metal cation (PMC) in solution, using a low-field benchtop TD-NMR relaxometer, focusing on analytical, electrochemical, and inorganic chemistry applications. Basic information on NMR and

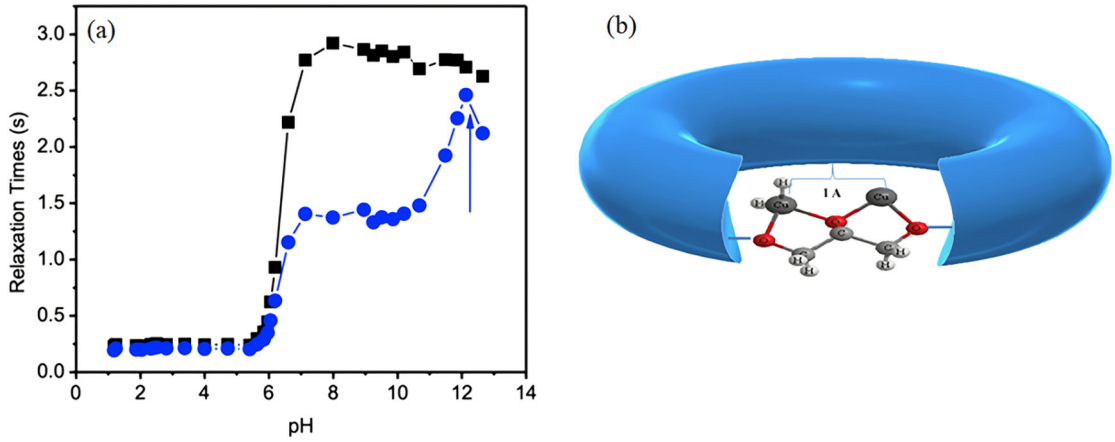

Figure 14. (a) T_1 (■) and T_2 (●) relaxometric profiles determined simultaneously with the CP-CWFP$_{x\text{-}x}$ pulse sequence for the aqueous solutions of 1:1 $[Cu^{II}\text{-Sorb}]$ complex, as a function of the pH; (b) proposed macromolecular arrangement for the $[Cu^{II}\text{-Sorb}]$ complex (reproduced from reference 87 with copyright permission of John Wiley & Sons, Ltd.).

Table 1. Potential uses of TD-NMR applied to PMC in solution

Year	Frequency / MHz (pulse sequence)	Application	Reference
2020	0.01-40.0 (IR)	quantification of Mn^{II} in wine	70
2020	0.01-70.0 (IR)	characterization of inorganic hybrid systems	91
2020	20.0 (IR and CPMG)	removal monitoring of Cu^{II} and Cr^{III} ions by amberlites	89
2019	20.0 (CP-$CWFP_{x-x}$)	study on supramolecular arrangements for PMC complexes	87
2019	34.0 (CPMG)	study on Cu^{II} electrodeposition using inductively coupled coils	74
2018	20.0 and 29.0 (SR and CPMG)	monitoring of Cu^{II} ions adsorption on activated alumina	90
2018	2.2 (CPMG)	quantification PMC in solution and comparison to optical emission spectrometry method	65
2017	20.0 (CP-$CWFP_{x-x}$)	studies on the interaction between PMC and biomacromolecules in solution	54
2016	0.01-40.0 (IR)	evaluation of the surface affinity of water in biochar containing PMC impurities	92
2016	9.7 and 14.2 (CPMG)	quantification of PMC in solution and comparison with other analytical methods	68
2015	10.0 (CPMG)	determination of solubility product constant for PMC in solution	69
2015	20.0 (CWFP and CP-CWFP)	rapid and simultaneous relaxometric approaches to study PMC in solution	41
2014	9.7 (CPMG)	*in situ* monitoring of Cu^{II} during an electrodeposition reaction	13
2012	42.3 (CPMG)	characterization of black heart diseases in pomegranate fruits	72
2012	9.0 (CPMG)	*in situ* quantification of Cu^{II} during an electrodeposition reaction	75
2012	0.5 (IR)	Mn^{II} binding evaluation to human serum albumin by relaxometry	67
2010	43.8 (CPMG)	paramagnetic ion uptake by onion samples for cell integrity studies	93
2007	1.0 (CPMG)	study on paramagnetic metal bond to a humic acid mixture	94
2007	0.01-20 (IR)	analysis of hydrated cement-based materials containing paramagnetic impurities	95
1978	20 (Echo Hahn)	study on complexometric reactions for PMC in solution	62
1978	20 (Echo Hahn)	NMR complexometric and precipitation titration for PMC in solution	63
1973	20 (Echo Hahn and CP)	NMR titration for PMC in solution	61
1970	20 (Echo Hahn and CP)	NMR titration for PMC in solution	60

IR: infrared; CPMG: Carr-Purcell sequence improved by Meiboom-Gill; CP-$CWFP_{x-x}$: Carr-Purcell continuous wave free precession with 180° phase shift alternation; PMC: paramagnetic metal cations; SR: saturation-recovery; NMR: nuclear magnetic resonance.

paramagnetic relaxation mechanism to understand data analysis, as well as of modern CWFP pulses sequences to measure both T_1 and T_2 relaxation times constants have been addressed. The use of bench top TD-NMR relaxometer is a viable cost-effective alternative to traditional, laborious, and expensive analytical approaches, such as ICP OES, and illustrates its contribution to analytical chemistry. Studies on copper electrodeposition reactions

and magnetohydrodynamic effect (MHD) demonstrated the potential of TD-NMR relaxometry to research on electrochemistry. Furthermore, the monitoring of PMC complexes and the coordination of compounds formation even for colorless ions and supramolecular arrangements for metal complexes confirm the remarkable contribution from the TD-NMR for inorganic chemistry. It also opens a new research path concerning these purposes with deep impact on the development of novel materials, environmental responses, and on the comprehension about interactions of metal-ligand chemical mechanisms in solution. Finally, we hope that the concepts and applications presented in this review pave the path for new applications of TD-NMR relaxometry using paramagnetic ion complexes in solution for all scientists.

Acknowledgments

The authors would like to thank the financial support of FAPESP (grants 2012/23169-8, 2015/16624-9, 2018/16040-5, 2019/13656-8 and 2021/12694-3) and CNPq (grant 302866/2017-5).

Flávio V. C. Kock *received his PhD (2018) in Chemistry, with expertise in Analytical and Inorganic Chemistry by the São Carlos Chemistry Institute of the University of São Paulo (USP). He has experience in the development and application of methods in nuclear magnetic resonance (NMR), with more than 20 papers published in high-impact scientific journals, patent deposits, and conferences abstracts covering the applications of NMR to coordination, bioinorganic, environmental, and analytical chemistry. In addition, Dr Kock received numerous national and international awards/distinctions, such as the national prize of the best thesis in the chemistry field.*

Luiz A. Colnago *received his PhD (1983) in Chemistry from the Military Institute of Engineering. He has been developing nuclear magnetic resonance (NMR) instrumentation, new pulse sequence and data processing methods and applications of NMR spectroscopy, NMR relaxometry and NMR imaging in analytical, organic, and inorganic chemistry, electrochemistry, biochemistry, metabolomics, fuel and biofuels, materials and biomaterials, and food. These results have been published in more than 200 scientific papers, book chapters and national and international patents.*

References

1. Aime, S.; Botta, M.; Fasano, M.; Terreno, E.; *Chem. Soc. Rev.* **1998**, *27*, 19.
2. Lammers, T.; Aime, S.; Hennink, W. E.; Storm, G.; Kiessling, F.; *Acc. Chem. Res.* **2011**, *44*, 1029.
3. Castelli, D. D.; Gianolio, E.; Crich, S. G.; Terreno, E.; Aime, S.; *Coord. Chem. Rev.* **2008**, *252*, 2424.
4. Terreno, E.; Uggeri, F.; Aime, S.; *J. Controlled Release* **2012**, *161*, 328.
5. Luchinat, C.; *Magn. Reson. Chem.* **1993**, *31*, S145.
6. Telser, J.; *J. Braz. Chem. Soc.* **2006**, *17*, 1501.
7. Helm, L.; *Prog. Nucl. Magn. Reson. Spectrosc.* **2006**, *49*, 45.
8. Pell, A. J.; Pintacuda, G.; Grey, C. P.; *Prog. Nucl. Magn. Reson. Spectrosc.* **2019**, *111*, 1.
9. Bertini, I.; Kowalewski, J.; Luchinat, C.; Nilsson, T.; Parigi, G.; *J. Chem. Phys.* **1999**, *111*, 5795.
10. Kellar, K. E.; Foster, N.; *Inorg. Chem.* **1992**, *31*, 1353.
11. Aime, S.; Baroni, S.; Castelli, D. D.; Brücher, E.; Fábián, I.; Serra, S. C.; Mingo, A. F.; Napolitano, R.; Lattuada, L.; Tedoldi, F.; Baranyai, Z.; *Inorg. Chem.* **2018**, *57*, 5567.
12. Helm, L.; Merbach, A. E.; *Chem. Rev.* **2005**, *105*, 1923.
13. Gomes, B. F.; Nunes, L. M. S.; Lobo, C. M. S.; Cabeça, L. F.; Colnago, L. A.; *Anal. Chem.* **2014**, *86*, 9391.
14. Gomes, B. F.; Lobo, C. M. S.; Colnago, L. A.; *Appl. Sci.* **2019**, *9*, 498.
15. Helm, L.; Merbach, A. E.; *Coord. Chem. Rev.* **1999**, *187*, 151.
16. Caravan, P.; *Acc. Chem. Res.* **2009**, *42*, 851.
17. Caravan, P.; Ellison, J. J.; McMurry, T. J.; Lauffer, R. B.; *Chem. Rev.* **1999**, *99*, 2293.
18. Caravan, P.; *Chem. Soc. Rev.* **2006**, *35*, 512.
19. Blümich, B.; Casanova, F.; Appelt, S.; *Chem. Phys. Lett.* **2009**, *477*, 231.
20. Softley, C. A.; Bostock, M. J.; Popowicz, G. M.; Sattler, M.; *J. Biomol. NMR* **2020**, *74*, 287.
21. Claridge, T. D. W.; *High-Resolution NMR Techniques in Organic Chemistry: Third Edition*; Elsevier Ltd.: Oxford, 2016.
22. Bloch, F.; Hansen, W. W.; Packard, M.; *Phys. Rev.* **1946**, *70*, 474.
23. Bloembergen, N.; Purcell, E. M.; Pound, R. V.; *Phys. Rev.* **1948**, *73*, 679.
24. Solomon, I.; *Phys. Rev.* **1955**, *99*, 559.
25. Bloembergen, N.; *J. Chem. Phys.* **1957**, *27*, 572.
26. Bloembergen, N.; Morgan, L. O.; *J. Chem. Phys.* **1961**, *34*, 842.
27. Debroye, E.; Parac-Vogt, T. N.; *Chem. Soc. Rev.* **2014**, *43*, 8178.
28. Zhang, Y.; Yeung, H. N.; O'Donnell, M.; Carson, P. L.; *J. Magn. Reson. Imaging* **1998**, *8*, 675.
29. Look, D. C.; Locker, D. R.; *Rev. Sci. Instrum.* **1970**, *41*, 250.

30. Haase, A.; Frahm, J.; *J. Magn. Reson.* **1985**, *65*, 481.
31. Datta, A.; Raymond, K. N.; *Acc. Chem. Res.* **2009**, *42*, 938.
32. Lamanna, R.; *Concepts Magn. Reson., Part A: Bridging Educ. Res.* **2005**, *26*, 78.
33. Berman, P.; Levi, O.; Parmet, Y.; Saunders, M.; Wiesman, Z.; *Concepts Magn. Reson., Part A* **2013**, *42*, 72.
34. Cucinelli Neto, R. P.; Rodrigues, E. J. R.; Tavares, M. I. B.; *Magn. Reson. Chem.* **2019**, *57*, 395.
35. Moraes, T. B.; Monaretto, T.; Colnago, L. A.; *J. Magn. Reson.* **2016**, *270*, 1.
36. Hahn, E. L.; *Phys. Rev.* **1950**, *80*, 580.
37. Carr, H. Y.; Purcell, E. M.; *Phys. Rev.* **1954**, *94*, 630.
38. Meiboom, S.; Gill, D.; *Rev. Sci. Instrum.* **1958**, *29*, 688.
39. de Andrade, F. D.; Netto, A. M.; Colnago, L. A.; *Talanta* **2011**, *84*, 84.
40. de Andrade, F. D.; Marchi Netto, A.; Colnago, L. A.; *J. Magn. Reson.* **2012**, *214*, 184.
41. Kock, F. V. C.; Colnago, L. A.; *Microchem. J.* **2015**, *122*, 144.
42. Azeredo, R. B. V.; Colnago, L. A.; Engelsberg, M.; *Anal. Chem.* **2000**, *72*, 2401.
43. Azeredo, R. B. V.; Colnago, L. A.; Souza, A. A.; Engelsberg, M.; *Anal. Chim. Acta* **2003**, *478*, 313.
44. Ernst, R. R.; Anderson, W. A.; *Rev. Sci. Instrum.* **1966**, *37*, 93.
45. Azeredo, R. B. V.; Engelsberg, M.; Colnago, L. A.; *Phys. Rev. E: Stat. Phys., Plasmas, Fluids, Relat. Interdiscip. Top.* **2001**, *64*, 4.
46. dos Santos, P. M.; de Souza, A. A.; Colnago, L. A.; *Appl. Magn. Reson.* **2011**, *40*, 331.
47. dos Santos, P. M.; de Souza, A. A.; Colnago, L. A.; *Quim. Nova* **2010**, *33*, 954.
48. Nunes, L. M. S.; Moraes, T. B.; Barbosa, L. L.; Mazo, L. H.; Colnago, L. A.; *Anal. Chim. Acta* **2014**, *850*, 1.
49. Moraes, T. B.; Monaretto, T.; Colnago, L. A.; *Appl. Sci.* **2019**, *9*, 1312.
50. Venâncio, T.; Colnago, L. A.; *Magn. Reson. Chem.* **2012**, *50*, 534.
51. Venâncio, T.; Engelsberg, M.; Azeredo, R. B. V.; Colnago, L. A.; *J. Magn. Reson.* **2006**, *181*, 29.
52. Monaretto, T.; Andrade, F. D.; Moraes, T. B.; Souza, A. A.; deAzevedo, E. R.; Colnago, L. A.; *J. Magn. Reson.* **2015**, *259*, 174.
53. Kock, F. V. C.; Colnago, L. A.; *Carbohydr. Polym.* **2016**, *150*, 1.
54. Kock, F. V. C.; Monaretto, T.; Colnago, L. A.; *Int. J. Biol. Macromol.* **2017**, *98*, 228.
55. Rondeau-Mouro, C.; Kovrlija, R.; Van Steenberge, E.; Moussaoui, S.; *J. Magn. Reson.* **2016**, *265*, 16.
56. Guo, J.; Xie, R.; *Appl. Magn. Reson.* **2019**, *50*, 479.
57. Monaretto, T.; Montrazi, E. T.; Moraes, T. B.; Souza, A. A.; Rondeau-Mouro, C.; Colnago, L. A.; *J. Magn. Reson.* **2020**, *311*, 106666.
58. Gianolio, E.; Stefania, R.; Di Gregorio, E.; Aime, S.; *Eur. J. Inorg. Chem.* **2012**, 1934.
59. Terreno, E.; Castelli, D. D.; Viale, A.; Aime, S.; *Chem. Rev.* **2010**, *110*, 3019.
60. Nothnagel, K. H.; Weiss, A.; *Ber. Bunsenges. Phys. Chem.* **1970**, *74*, 609.
61. Schlüter, A.; Weiss, A.; *Fresenius' Z. Anal. Chem.* **1973**, *266*, 177.
62. Schlüter, A.; Weiss, A.; *Anal. Chim. Acta* **1978**, *99*, 157.
63. Schlüter, A.; Weiss, A.; *Anal. Chim. Acta* **1978**, *97*, 93.
64. Aime, S.; Cabella, C.; Colombatto, S.; Crich, S. G.; Gianolio, E.; Maggioni, F.; *J. Magn. Reson. Imaging* **2002**, *16*, 394.
65. Kock, F. V. C.; Machado, M. P.; Athayde, G. P. B.; Colnago, L. A.; Barbosa, L. L.; *Microchem. J.* **2018**, *137*, 204.
66. Que, E. L.; Gianolio, E.; Baker, S. L.; Wong, A. P.; Aime, S.; Chang, C. J.; *J. Am. Chem. Soc.* **2009**, *131*, 8527.
67. Fanali, G.; Cao, Y.; Ascenzi, P.; Fasano, M.; *J. Inorg. Biochem.* **2012**, *117*, 198.
68. Gomes, B. F.; Burato, J. S. D. S.; Lobo, C. M. S.; Colnago, L. A.; *Int. J. Anal. Chem.* **2016**, *2016*, 8256437.
69. Cobra, P. F.; Gomes, B. F.; Mitre, C. I. N.; Barbosa, L. L.; Marconcini, L. V.; Colnago, L. A.; *Microchem. J.* **2015**, *121*, 14.
70. Bodart, P. R.; Rachocki, A.; Tritt-Goc, J.; Michalke, B.; Schmitt-Kopplin, P.; Karbowiak, T.; Gougeon, R. D.; *Talanta* **2020**, *209*, 120561.
71. Besghini, D.; Mauri, M.; Simonutti, R.; *Appl. Sci.* **2019**, *9*, 1801.
72. Zhang, L.; McCarthy, M. J.; *Postharvest Biol. Technol.* **2012**, *67*, 96.
73. Barbosa, L. L.; Colnago, L. A.; Carlos, I.; Nunes, L. M. S.; *ECS Trans.* **2010**, *25*, 215.
74. Lobo, C. M. S.; Gomes, B. F.; Bouzouma, H.; Danieli, E.; Blümich, B.; Colnago, L. A.; *Electrochim. Acta* **2019**, *298*, 844.
75. Nunes, L. M. S.; Cobra, P. F.; Cabeça, L. F.; Barbosa, L. L.; Colnago, L. A.; *Anal. Chem.* **2012**, *84*, 6351.
76. Gomes, B. F.; Nunes, L. M. S.; Lobo, C. M. S.; Carvalho, A. S.; Cabeça, L. F.; Colnago, L. A.; *J. Magn. Reson.* **2015**, *261*, 83.
77. Homsy, A.; Linder, V.; Lucklum, F.; de Rooij, N. F.; *Sens. Actuators, B* **2007**, *123*, 636.
78. Benders, S.; Gomes, B. F.; Carmo, M.; Colnago, L. A.; Blümich, B.; *J. Magn. Reson.* **2020**, *312*, 3.
79. Oakes, J.; Smith, E. G.; *J. Chem. Soc., Faraday Trans. 2* **1981**, *77*, 299.
80. Hernández, R. B.; Franco, A. P.; Yola, O. R.; López-Delgado, A.; Felcman, J.; Recio, M. A. L.; Mercê, A. L. R.; *J. Mol. Struct.* **2008**, *877*, 89.
81. Azarova, Y. A.; Pestov, A. V.; Ustinov, A. Y.; Bratskaya, S. Y.; *Carbohydr. Polym.* **2015**, *134*, 680.
82. Borsagli, F. G. L. M.; Mansur, A. A. P.; Chagas, P.; Oliveira, L. C. A.; Mansur, H. S.; *React. Funct. Polym.* **2015**, *97*, 37.

83. Webster, A.; Halling, M. D.; Grant, D. M.; *Carbohydr. Res.* **2007**, *342*, 1189.
84. Conte, P.; *Magn. Reson. Chem.* **2015**, *53*, 711.
85. Pinho, S. L. C.; Pereira, G. A.; Voisin, P.; Kassem, J.; Bouchaud, V.; Etienne, L.; Peters, J. A.; Carlos, L.; Mornet, S.; Geraldes, C. F. G. C.; Rocha, J.; Delville, M. H.; *ACS Nano* **2010**, *4*, 5339.
86. Klüfers, P.; Schuhmacher, J.; *Angew. Chem., Int. Ed. Engl.* **1995**, *34*, 2119.
87. Kock, F. V. C.; Higuera-Padilla, A. R.; Vigatto, M. D. S. S.; Martin Neto, L.; Colnago, L. A.; *Magn. Reson. Chem.* **2019**, *57*, 404.
88. Niu, X.; Dong, J.; Wang, X. L.; Yao, Y. F.; *Environ. Sci. Nano* **2020**, *7*, 2823.
89. Gossuin, Y.; Hantson, A. L.; Vuong, Q. L.; *J. Water Process Eng.* **2020**, *33*, 101024.
90. Gossuin, Y.; Vuong, Q. L.; *Sep. Purif. Technol.* **2018**, *202*, 138.
91. Lalli, D.; Marchesi, S.; Carniato, F.; Bisio, C.; Tei, L.; Marchese, L.; Botta, M.; *Dalton Trans.* **2020**, *49*, 6566.
92. Bubici, S.; Korb, J. P.; Kučerik, J.; Conte, P.; *Magn. Reson. Chem.* **2016**, *54*, 365.
93. Ersus, S.; Oztop, M. H.; McCarthy, M. J.; Barrett, D. M.; *J. Food Sci.* **2010**, *75*, E444.
94. Melton, J. R.; Kantzas, A.; Langford, C. H.; *Anal. Chim. Acta* **2007**, *605*, 46.
95. Korb, J. P.; Monteilhet, L.; McDonald, P. J.; Mitchell, J.; *Cem. Concr. Res.* **2007**, *37*, 295.

Submitted: October 27, 2021
Published online: March 11, 2022